AIAA JOURNAL
Vol. 39, No. 3, March 2001

Modeling Segmented Active Constrained Layer Damping Using Hybrid Displacement Field

Aditi Chattopadhyay,* Haozhong Gu,† and Rajan Beri‡
Arizona State University, Tempe, Arizona 85287-6106
and
Changho Nam§
Arizona State University East, Mesa, Arizona 85212

A finite element model for composite plates with active constrained layer damping is developed using hybrid displacement fields. The higher-order displacement field is used in the composite plate to capture the transverse shear deformations. Because viscoelastic layer and piezoelectric layers are made from certain isotropic materials, the first- and the second-order displacement fields are employed in these layers to maintain computational efficiency in solving the problem. The refined displacement fields defined in different material layers are derived by applying the displacement and transverse shear stress continuity conditions at the interfaces of different materials and the traction-free boundary conditions at the top and the bottom surfaces of the structure. The inelastic displacement field method is used to implement the viscoelastic material model to enable time-domain finite element analysis. The finite element model is correlated through NASTRAN-3D finite element static and modal analysis. Detailed numerical studies are presented to assess the influence of number of actuators and their locations for vibration control.

Introduction

ACTIVE constrained layer (ACL) damping configuration capitalizes on both passive and active damping techniques in a synergistic manner and has been shown to be an effective method for vibration suppression in composite structures.[1−3] The primary concern in such a configuration is the concept that the actuation ability of the piezoelectric layer is reduced by the viscoelastic layer. However, the active constraining layer (piezoelectric layer) increases the shear deformation in the viscoelastic layer and, therefore, in reality forms an effective means of enhancing the damping mechanism.

ACL damping treatment has recently received significant attention, as summarized by Ro and Baz.[1] Baz and Ro derived the equations for partial treatment of a beam[2] and employed the finite element method for the same system.[3] Van Norstrand and Inman[4] extended the beam finite element model to capture the frequency-dependent behavior of viscoelastic material using augmenting thermodynamic fields (ATF) time-domain modeling method.[5] Later, Lam et al.[6] used the Golla–Hughes–McTavish approach to model the active constrained layer. In a series of papers,[7−10] Shen investigated several aspects of ACL damping treatments with emphasis on performance, controllability, and stability. Azvine et al.[11] considered a cantilever beam with velocity feedback in which the piezoelectric actuator is bonded to (not replacing) the constraining layer. Liao and Wang[12,13] used modern control theory to examine the hybrid nature of the ACL damping treatment. Most of the ACL damping models mentioned are beam models, and they are generally addressed by using a single ACL that covers the entire surface of the structure. It is well known that segmented constraining layer is an effective means of increasing passive damping in long wavelength vibration modes by increasing the number of high shear regions. Lesieutre and Lee[14] explored segmented configuration in the ACL damping treatment. They found that, in addition to the passive benefits, segmentation provided the possibility of additional independent control inputs to improve the structural performance. However, the segmented constraining layers presented in their paper still covered the entire surface of the structure and, therefore, does not represent a realistic configuration for engineering practice.

Based on researches reported in the literature, several issues still need to be addressed in modeling composite structures with ACL damping. First, the significance of transverse shear effects in the host composite structure needs to be considered. Second, a practical approach must be developed to model the sparse segmented ACL damping treatment. The development of such a general approach involves several complexities. These include those associated with boundary conditions that are necessary to solve for the additional variables introduced to describe the behavior of the viscoelastic layer. Moreover, the three different materials exhibit very different behavior in practical applications. The viscoelastic layer undergoes not only pure shear, but also extension (or compression) and bending. All of these issues need to be carefully examined.

To address these issues in composite plates with ACL damping, a new hybrid-displacement-field-based theory is developed. Three different displacement fields are assumed to describe the mechanical deformation in the three different material regions. The higher-order displacement field is used in the composite plate region to capture the significant transverse shear effects that are present in composites. The first- and the second-order displacement fields are used in the viscoelastic layer and the piezoelectric layer, respectively, to include shear effects while maintaining computational efficiency in the solution. The refined displacement fields defined in different materials are derived by applying the displacement and transverse shear stress continuity conditions at interfaces of different materials and the traction-free boundary conditions at the top and the bottom surfaces of the structure. A finite element approach is then developed based on these hybrid displacement fields. The approach is validated using results from NASTRAN-3D finite element analysis. A control system is designed for vibration suppression using a pole placement technique.

Displacement Field

A composite plate of arbitrary thickness with segmented viscoelastic layer and piezoelectric constraining layer is considered (Fig. 1). To model such a structure, the plate system is divided through the plate plain into two sections: section 1, plate without

Received 8 January 2000; revision received 7 September 2000; accepted for publication 15 October 2000.

*Professor, Department of Mechanical and Aerospace Engineering. Associate Fellow AIAA.
†Postdoctoral Research Associate, Department of Mechanical and Aerospace Engineering. Member AIAA.
‡Graduate Research Associate, Department of Mechanical and Aerospace Engineering. Member AIAA.
§Associate Professor, Manufacturing and Aeronautical Engineering Technology. Senior Member AIAA.

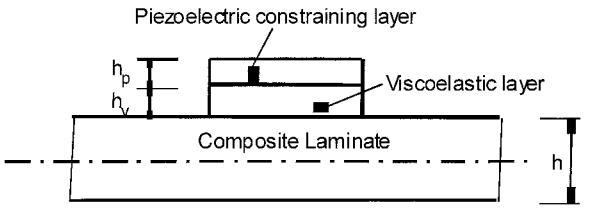

Fig. 1 ACL configuration.

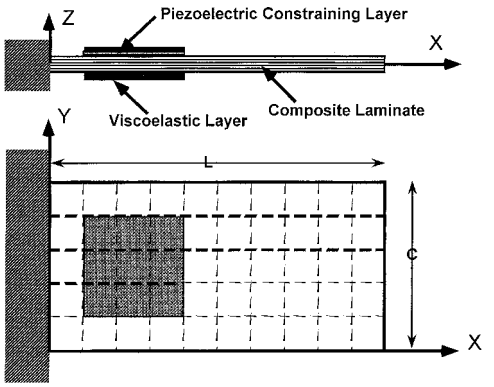

Fig. 2 Geometry and finite element model of the composite laminate with ACLs.

viscoelastic layer and the piezoelectric constraining layer, and section 2, plate with viscoelastic layer and piezoelectric constraining layer. In section 2, the plate system is separated further through the thickness into three different regions: composite region (region c), viscoelastic region (region v), and piezoelectric region (region p). A hybrid displacement field is developed to model the plate deformation in section 2, which is compatible with the unified third-order displacement field defined in section 1. A general higher-order displacement field is applied to the composite region to model accurately the transverse shear effects. The in-plane displacements are assumed to be effectively expressed by a cubic function through the thickness z and the transverse displacement is assumed to be independent of z. The general displacement field in the composite region (region c) is defined as follows:

$$u_1^c(x,y,z) = u_0^c(x,y) - zw_{0,x}^c(x,y) + z\psi_x^c(x,y) + z^2\varphi_x^c(x,y) + z^3\phi_x^c(x,y)$$

$$u_2^c(x,y,z) = v_0^c(x,y) - zw_{0,y}^c(x,y) + z\psi_y^c(x,y) + z^2\varphi_y^c(x,y) + z^3\phi_y^c(x,y)$$

$$u_3^c(x,y,z) = w_0^c(x,y) \tag{1}$$

where u, v, and w are the in-plane and the out-of-plane displacements at a point (x, y, z); u_0, v_0, and w_0 are the displacements at the midplane, and ψ_x and ψ_y are the rotations of the normals to the midplane. The quantities φ_x, φ_y, ϕ_x, and ϕ_y are the higher-order terms. The superscript c denotes variables defined in the composite region only. The comma denotes partial differentiation with respect to the index that follows. The coordinate system used for the formulation is presented in Fig. 2. Because the viscoelastic layer is made of isotropic material, the transverse shear effect in this region is expected to be much smaller compared to that in the composite region. To simplify the current model while making it compatible with composite region, the first-order displacement field is used in this region:

$$u_1^v(x,y,z) = u_0^v(x,y) - zw_{0,x}^v(x,y) + z\psi_x^v(x,y)$$

$$u_2^v(x,y,z) = v_0^v(x,y) - zw_{0,y}^v(x,y) + z\psi_y^v(x,y)$$

$$u_3^v(x,y,z) = w_0^v(x,y) \tag{2}$$

where the superscript v denotes variables defined in the viscoelastic region. For the piezoelectric region, the second-order displacement field is used to ensure the applicability of boundary conditions at the piezoelectric layer outer surface:

$$u_1^p(x,y,z) = u_0^p(x,y) - zw_{0,x}^p(x,y) + z\psi_x^p(x,y) + z^2\varphi_x^p(x,y)$$

$$u_2^p(x,y,z) = v_0^p(x,y) - zw_{0,y}^p(x,y) + z\psi_y^p(x,y) + z^2\varphi_y^p(x,y)$$

$$u_3^p(x,y,z) = w_0^p(x,y) \tag{3}$$

where the superscript p denotes variables defined in the piezoelectric region.

The continuity conditions must be satisfied at region interfaces. These continuity conditions require that the displacements u, v, and w and the transverse shear stresses τ_{xz} and τ_{yz} defined at adjacent region be equal to each other at their interface. For multilayered laminates made up of layers of orthotropic or isotropic lamina, this is equivalent to the requirement that the displacements and the corresponding strains ε_{xz} and ε_{yz} be equal at these interfaces. These can be expressed in terms of displacements as follows:

$$u_1^c = u_1^v, \qquad u_2^c = u_2^v, \qquad u_3^c = u_3^v, \qquad z = h/2$$

$$u_1^v = u_1^p, \qquad u_2^v = u_2^p, \qquad u_3^v = u_3^p, \qquad z = h/2 + h_v \tag{4}$$

$$G_{13}^c\left(u_{1,z}^c + u_{3,x}^c\right) = G^v\left(u_{1,z}^v + u_{3,x}^v\right)$$

$$G_{23}^c\left(u_{2,z}^c + u_{3,y}^c\right) = G^v\left(u_{2,z}^v + u_{3,y}^v\right), \qquad z = h/2$$

$$G^v\left(u_{1,z}^v + u_{3,x}^v\right) = G^p\left(u_{1,z}^p + u_{3,x}^p\right)$$

$$G^v\left(u_{2,z}^v + u_{3,y}^v\right) = G^p\left(u_{2,z}^p + u_{3,y}^p\right), \qquad z = h/2 + h_v \tag{5}$$

where the quantities h, h_v, and h_p are the thicknesses of the composite plate, the viscoelastic layer, and the piezoelectric layer, respectively. The boundary conditions also require that the transverse shear stresses τ_{xz} and τ_{yz} vanish at the top and bottom surfaces of the plate. The displacement expressions of the boundary conditions are

$$u_{1,z}^c + u_{3,x}^c = 0, \qquad u_{2,z}^c + u_{3,y}^c = 0, \qquad z = -h/2$$

$$u_{1,z}^p + u_{3,x}^p = 0, \qquad u_{2,z}^p + u_{3,y}^p = 0, \qquad z = h/2 + h_v + h_p \tag{6}$$

Using Eqs. (4–6), the 14 variables defined in Eqs. (1–3) are determined in terms of the remaining 7 variables that are independent. It can be shown that the original three displacement fields are reduced to the following set of equations:

$$u_1^c = u_0^c - zw_{0,x}^c + z\left(1 - \frac{4z^2}{3h^2}\right)\psi_x^c + \frac{2z^2}{3h^2}\left(z + \frac{3}{4}h\right)\frac{G^v}{G_{13}^c}\psi_x^v$$

$$u_2^c = v_0^c - zw_{0,y}^c + z\left(1 - \frac{4z^2}{3h^2}\right)\psi_y^c + \frac{2z^2}{3h^2}\left(z + \frac{3}{4}h\right)\frac{G^v}{G_{23}^c}\psi_y^v$$

$$u_3^c = w_0^c, \qquad \text{where } -\frac{h}{2} \le z \le \frac{h}{2} \tag{7a}$$

$$u_1^v = u_0^c + \frac{h}{3}\psi_x^c - zw_{0,x}^c + \left(z - \frac{h}{2} + \frac{5h}{24}\frac{G^v}{G_{13}^c}\right)\psi_x^v$$

$$u_2^v = v_0^c + \frac{h}{3}\psi_y^c - zw_{0,y}^c + \left(z - \frac{h}{2} + \frac{5h}{24}\frac{G^v}{G_{23}^c}\right)\psi_y^v$$

$$u_3^v = w_0^c, \qquad \text{where } \frac{h}{2} \le z \le \frac{h}{2} + h_v \tag{7b}$$

$$u_1^p = u_0^c + \frac{h}{3}\psi_x^c - zw_{0,x}^c + \left[\frac{G^v}{G^p}\frac{1}{2h_p}\left(2h_4 z - z^2 - h_3h_4 - h_3h_p\right) + h_v + \frac{5h}{24}\frac{G^v}{G_{13}^c}\right]\psi_x^v$$

$$u_2^p = v_0^c + \frac{h}{3}\psi_y^c - zw_{0,y}^c + \left[\frac{G^v}{G^p}\frac{1}{2h_p}\left(2h_4 z - z^2 - h_3h_4 - h_3h_p\right) + h_v + \frac{5h}{24}\frac{G^v}{G_{23}^c}\right]\psi_y^v$$

$$u_3^p = w_0^c, \qquad \text{where } \frac{h}{2} + h_v \le z \le \frac{h}{2} + h_v + h_p \tag{7c}$$

with

$$h_3 = h/2 + h_v, \qquad h_4 = h/2 + h_v + h_p \tag{8}$$

where G is the shear moduli of the material. The application of transverse shear stress continuity conditions [Eq. (5)] at the interface between the composite and the viscoelastic layer and the interface between the viscoelastic layer and the piezoelectric layer lead to the appearance of the terms G^v/G^c and G^v/G^p in Eq. (7). The present approach is able to model accurately the varying behaviors in the different material regions. It also has the advantage of having less unknown variables in the formulation (only two additional variables, ψ_x^v and ψ_y^v, compared to the regular refined third-order theory), while satisfying all boundary and continuity conditions. An added benefit is that the boundary conditions for the two additional unknowns ψ_x^v and ψ_y^v, defined in the segmented constraining layer, can be derived using the present approach. To determine these two additional unknowns, the regular refined third-order displacement field used in section 1 (section without viscoelastic layer and the piezoelectric constraining layer) is presented:

$$u_1^c = u_0^c - zw_{0,x}^c + z\left(1 - \frac{4z^2}{3h^2}\right)\psi_x^c + \frac{2z^2}{3h^2}\left(z + \frac{3}{4}h\right)\frac{G^v}{G_{13}^c}\psi_x^v$$

$$u_2^c = v_0^c - zw_{0,y}^c + z\left(1 - \frac{4z^2}{3h^2}\right)\psi_y^c + \frac{2z^2}{3h^2}\left(z + \frac{3}{4}h\right)\frac{G^v}{G_{23}^c}\psi_y^v$$

$$u_3^c = w_0^c, \qquad \text{where} -\frac{h}{2} \le z \le \frac{h}{2} \tag{9}$$

The continuity conditions at section interfaces require that the displacements defined in adjacent sections [Eqs. (7) and (9)] be equal to each other through the thickness. These lead to the solution

$$\psi_x^v(x, y) = \psi_y^v(x, y) = 0, \qquad (x, y) \in \Gamma_s \tag{10}$$

where Γ_s is the section interface.

Finite Element Model

The finite element method (FEM) is used to implement the present hybrid displacement fields because it allows for the analysis of practical geometries and boundary conditions. Based on the displacement field [Eq. (7)], the strain vector for an element with viscoelastic damping layer and piezoelectric actuator layer in section 2 can be expressed as

$$\{\varepsilon\} = \begin{cases} \{\varepsilon^c\} & -h/2 \le z \le h/2 \\ \{\varepsilon^v\} & h/2 \le z \le h/2 + h_v \\ \{\varepsilon^p\} & h/2 \le z \le h/2 + h_v + h_p \end{cases} \qquad (x, y) \in \Sigma_2 \tag{11}$$

where Γ_s is section 2 area. The finite element equations are derived using the discretized form of Hamilton's principle, which is stated as follows:

$$\begin{aligned} \delta\Pi &= \int_t (\delta K - \delta U - \delta W)\,\mathrm{d}t \\ &= \int_t \int_A \int_z [\delta\{u\}^T[\rho]\{\ddot{u}\} - \delta\{\varepsilon\}^T[\bar{Q}](\{\varepsilon\} - \{\Lambda\})]\,\mathrm{d}z\,\mathrm{d}A\,\mathrm{d}t \\ &\quad - \int_t \int_A \delta\{u\}^T\{q\}\,\mathrm{d}A\,\mathrm{d}t \\ &= 0 \end{aligned} \tag{12}$$

where $\{u\}$ is the displacement vector, $[\rho]$ is material density coefficient matrix, $[\bar{Q}]$ is material stiffness matrix, $\{\Lambda\}$ is piezoelectric induced strain vector, and $\{q\}$ is the applied external distributed forces on plate surfaces. The overdot denotes differentiation with respect to time t. The element stiffness matrix, the mass matrix, the discretized displacement vector, the piezoelectric force vector, and the external force vector can be expressed as follows:

$$\{u\} = [N^e]\{u^e\}, \qquad \{\varepsilon\} = [L^e][N^e], \qquad \{u^e\} = [B^e]\{u^e\}$$

$$[K^e] = \int_A \int_z [B^e]^T[\bar{Q}^e][B^e]\,\mathrm{d}A\,\mathrm{d}z$$

$$[M^e] = \int_A \int_z [N^e]^T[\rho^e][N^e]\,\mathrm{d}A\,\mathrm{d}z$$

$$\left\{f_p^e\right\} = \int_A [B^e]^T\{\Lambda\}\,\mathrm{d}A, \qquad \{f^e\} = \int_A [N^e]^T\{q\}\,\mathrm{d}A \tag{13}$$

where superscript e denotes the discretized elemental quantities, $[L^e]$ is the operator matrix, and $[N^e]$ is the interpolation function matrix. As shown in Eq. (11), the stiffness and mass matrices defined in section 2 can be divided into three components corresponding to the three different regions:

$$[K^e] = \left[K_c^e\right] + \left[K_v^e\right] + \left[K_p^e\right]$$

$$[M^e] = \left[M_c^e\right] + \left[M_v^e\right] + \left[M_p^e\right] \tag{14}$$

The global finite element equations of motion are then expressed as follows:

$$[M_g]\{\ddot{u}_g\} + [K_g]\{u_g\} = \{F_g\} + \left\{F_g^p\right\} \tag{15}$$

where subscript g denotes the discretized global quantities.

The anelastic displacement field method[14] is used to implement the viscoelastic material model to enable time-domain finite element analysis. In this approach, the total deformation (both normal and shear) defined in the viscoelastic material is divided into two parts: 1) an elastic component in which the strain is instantaneously proportional to the stress and 2) an anelastic component that captures the characteristic relaxation behavior:

$$\left\{u_t^v\right\} = \left\{u_e^v\right\} + \left\{u_a^v\right\} \tag{16}$$

where $\{u_t^v\}$, $\{u_e^v\}$, and $\{u_a^v\}$ are the total displacements, their elastic components, and their anelastic components, respectively. In Hamilton's principle, only elastic strain can be taken into account. Therefore, the strain $\{\varepsilon^v\}$ used in Eq. (12) should be replaced by its elastic component as follows:

$$\left\{\varepsilon_e^v\right\} = \left\{\varepsilon_t^v\right\} - \left\{\varepsilon_a^v\right\} \tag{17}$$

Then, Eqs. (14) and (15) can be rewritten as follows:

$$[K^e] = \left[K_c^e\right] + \left[K_v^e\right] + \left[K_p^e\right] - \left[K_{va}^e\right]$$

$$[M^e] = \left[M_c^e\right] + \left[M_v^e\right] + \left[M_p^e\right] \tag{18}$$

$$[M_g]\{\ddot{u}_g\} + [K_g]\{u_g\} - [K_{gv}]\{u_v\} = \{F_g\} + \left\{F_g^p\right\} \tag{19}$$

where $[K_{va}^e]$ is the additional element stiffness matrix corresponding to anelastic strain, and $[K_{gv}]$ and $\{u_v\}$ are the additional global

stiffness matrices corresponding to the anelastic strain in elastic equations and global discretized displacement vector corresponding to the anelastic displacement components, respectively.

An additional set of ordinary differential equations[14] that describe the time evolution of the anelastic displacement fields is employed to obtain the solution of the complete system:

$$(c/\Omega)[K_v]\{\dot{u}_v\} - [K_{vg}]\{u_g\} + c[K_v]\{u_v\} = \{0\} \tag{20}$$

where $[K_v]$ is the global stiffness matrix constituting anelastic strain and c and Ω are material constitutive coupling parameter and characteristic relaxation time at constant strain, respectively. The final global equations of motion for the complete ACL structure are written as follows:

$$\begin{bmatrix}[M_g] & [0]\\ [0] & [0]\end{bmatrix}\begin{Bmatrix}\{\ddot{u}_g\}\\ \{\ddot{u}_v\}\end{Bmatrix} + \begin{bmatrix}[0] & [0]\\ [0] & (c/\Omega)[K_v]\end{bmatrix}\begin{Bmatrix}\{\dot{u}_g\}\\ \{\dot{u}_v\}\end{Bmatrix}$$
$$+ \begin{bmatrix}[K_g] & -[K_{gv}]\\ -[K_{gv}]^T & c[K_v]\end{bmatrix}\begin{Bmatrix}\{u_g\}\\ \{u_v\}\end{Bmatrix} = \begin{Bmatrix}\{F_g^p\}\\ \{0\}\end{Bmatrix} \tag{21}$$

To simplify the solution process, the external force vector is removed from Eq. (21).

Active Control System Design

The eigenstructure assignment regulator theory is employed to suppress vibration with the smallest control effort. It is assumed that all states are available for feedback. Consider the completely controllable and observable linear dynamic system in the state-space form

$$\{\dot{x}\} = [A]\{x\} + [B]\{u\} \tag{22}$$

with linear feedback control

$$\{u\} = -[K_G]\{x\} \tag{23}$$

The right and left eigenvalue problems of the closed-loop system can be written, respectively, as

$$([A] - [B][K_G])\{\phi^c\}_i = \lambda_i^c\{\phi^c\}_i$$
$$([A] - [B][K_G])^T\{\psi^c\}_i = \lambda_i^c\{\psi^c\}_i \tag{24}$$

where $\{\phi^c\}_i$ and $\{\psi^c\}_i$ are the right and left eigenvectors of the closed-loop system, respectively, corresponding to the eigenvalue λ_i^c. The subscripts i refer to the variables related to the ith eigenvalue. The conventional normalization of biorthogonality conditions for the eigenvectors is adopted and is expressed as

$$\{\phi^c\}_i^T\{\phi^c\}_i = 1 \tag{25}$$

$$\{\psi^c\}_i^T\{\psi^c\}_i = 1 \tag{26}$$

In this study, the desired closed-loop eigenvalues are chosen based on the open-loop eigenvalues λ_i^0.

The pole placement algorithm based on Sylvester equation utilizes the parameter vector $\{h\}_i$ defined as follows[15]:

$$\{h\}_i = [K_G]\{\phi^c\}_i \tag{27}$$

Substituting Eq. (27) into Eq. (24) yields the following Sylvester equation:

$$\big([A] - \lambda_i^c[I]\big)\{\phi^c\}_i = [B]\{h\}_i \tag{28}$$

or in matrix form

$$[A][\Phi_c] - [\Phi_c][\Lambda_D] = [B][H] \tag{29}$$

where

$$[\Phi_c] = \big[\{\phi^c\}_1, \{\phi^c\}_2, \ldots, \{\phi^c\}_n\big]$$
$$[\Lambda_D] = \operatorname{diag}\big(\lambda_1^c,\ \lambda_2^c, \ldots, \lambda_n^c\big), \qquad [H] = [\{h\}_1, \{h\}_2, \ldots, \{h\}_n] \tag{30}$$

and $[\Lambda_D]$ contains the desired closed-loop eigenvalues. From Eq. (28), it can be seen that

$$\{\phi^c\}_i = \big([A] - \lambda_i^c[I]\big)^{-1}[B]\{h\}_i \tag{31}$$

If λ_i^c are distinct from their open-loop positions, the columns of $[H]$ generate the corresponding closed-loop eigenvectors. For the given parameter matrix $[H]$, the closed-loop modal matrix $[\Phi_c]$ can be determined by solving the Sylvester equation.

The important steps of the robust eigenstructure assignment algorithm[16,17] for vibration control are outlined next. First, a target eigenvector $[\Phi_T]$ is selected. In vibration control problems, it is known that the open-loop eigenvectors are well conditioned and are, therefore, a good choice of a family of admissible target vectors.[18] The open-loop eigenvectors are adopted as the target eigenvectors in this study. Second, $[H]$ matrix is computed by solving the Sylvester equation [Eq. (29)], in a least-square sense as follows:

$$[H] = [B]^*([A][\Phi_T] - [\Phi_T][\Lambda_D]) \tag{32}$$

where $[B]^*$ is the pseudoinverse of the matrix $[B]$. Next, the Sylvster equation is solved to obtain the closed-loop eigenvector matrix $[\Phi_c]$. Finally, the gain matrix is computed using Eq. (27) as follows:

$$[K_G] = [H][\Phi_c]^{-1} \tag{33}$$

Numerical Results and Discussion

To validate the hybrid displacement field theory, the developed finite element model is correlated through NASTRAN-3D finite element analysis. The comparisons are made for $[45/-45/45/-45\ \text{deg}]_s$ graphite/epoxy composites with ACL damping treatment on the top surface (Fig. 2). Static and modal analyses are conducted for the undamped system. The plate is clamped (through the width) along one side, and the other three sides are free. The material properties used in all examples are listed in Table 1. Eight noded brick elements are used in the NASTRAN-3D finite element model. The mesh sizes are as follows: a $100 \times 50 \times 8$ mesh is used in the composite regions, a $30 \times 30 \times 2$ mesh is used in the viscoelastic damping layer, and a $30 \times 30 \times 2$ mesh is used for the piezoelectric actuator layer.

The static solutions are obtained for two cases: case 1, an undamped plate with dimensions $a = 4$ m, $b = 1$ m, $h_c = 0.1$ m, $h_v = 0.0127$ m, and $h_p = 0.0254$ m; and case 2, an undamped plate with $a = 4$ m, $b = 1$ m, $h_c = 0.2$ m, $h_v = 0.0254$ m, and $h_p = 0.0508$ m (Fig. 2). A uniformly distributed tip load of 6 N/m is applied to the plate along the z direction (Fig. 2). For case 1 ($l/h_c = 40$), the corresponding three-dimensional NASTRAN stresses are compared with the present model, through the thickness z of the plate, in a region with ACL (at location $x = 0.6$ m and $y = 0.5$ m). Comparisons of the normal stresses σ_x and σ_y are presented in Figs. 3 and 4, respectively. As is evident from Figs. 3 and 4, the results from the present approach correlate very well with the NASTRAN solutions. The shear stresses σ_{xz} and σ_{yz} are presented in Figs. 5 and 6,

Table 1 Material properties of PZT and graphite/epoxy composite

Property	PZT	Viscoelastic layer	Graphite/epoxy
E_{11}, GPa	63	25	144.23
E_{22}, GPa	63	25	9.65
E_{33}, GPa	63	25	9.65
G_{23}, GPa	24.6	10	3.45
G_{13}, GPa	24.6	10	4.14
G_{12}, GPa	24.6	10	4.14
ν_{12}	0.28	0.25	0.3
ν_{23}	0.28	0.25	0.3
ν_{31}	0.28	0.25	0.02
Density, kg/m^3	7600	1600	1389.23
Piezoelectric constant			
$d_{31} = d_{32}$ pm/V	254		
Viscoelastic material			
Ω, rad/s		50	
c		1.2	

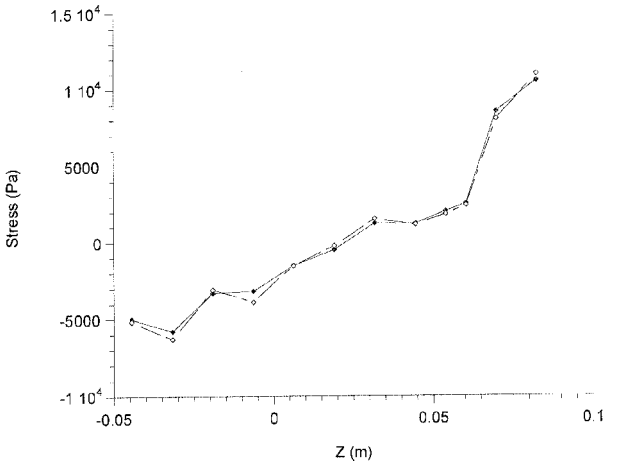

Fig. 3 Variation of normal stress σ_x with thickness, case 1: ♦, hybrid model, and ◇, NASTRAN-3D.

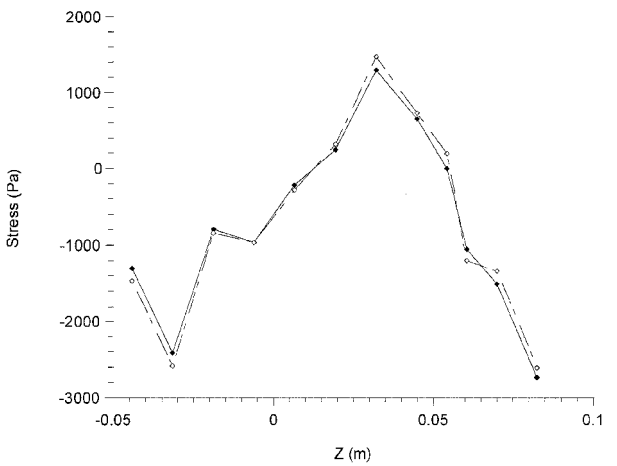

Fig. 4 Variation of normal stress σ_y with thickness, case 1: ♦, hybrid model, and ◇, NASTRAN-3D.

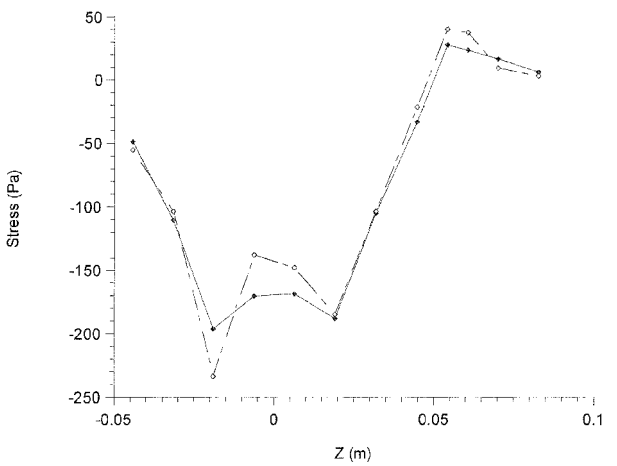

Fig. 5 Variation of shear stress σ_{xz} with thickness, case 1: ♦, hybrid model, and ◇, NASTRAN-3D.

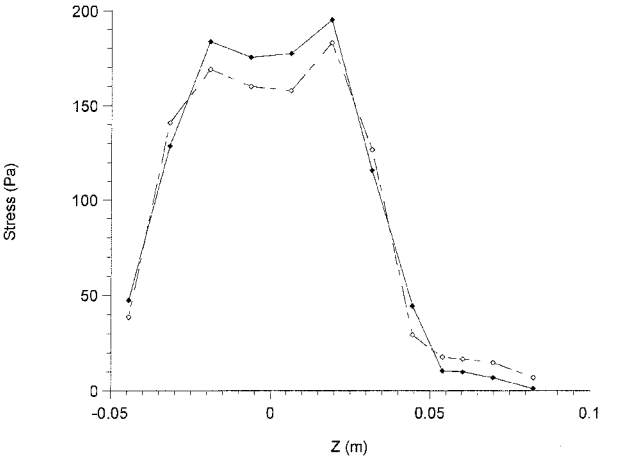

Fig. 6 Variation of shear stress σ_{yz} with thickness, case 1: ♦, hybrid model, and ◇, NASTRAN-3D.

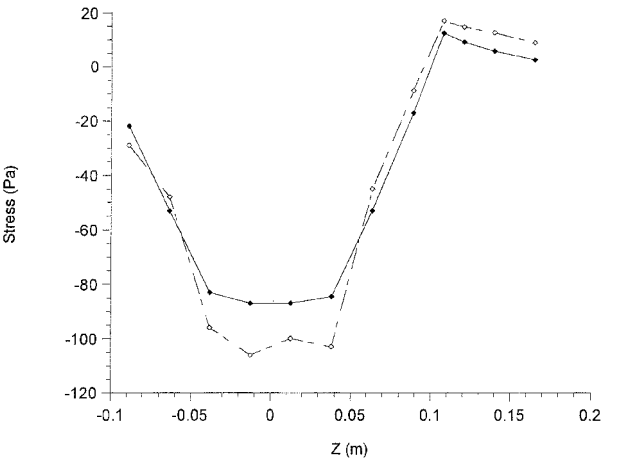

Fig. 7 Variation of shear stress σ_{xz} with thickness, case 2: ♦, hybrid model, and ◇, NASTRAN-3D.

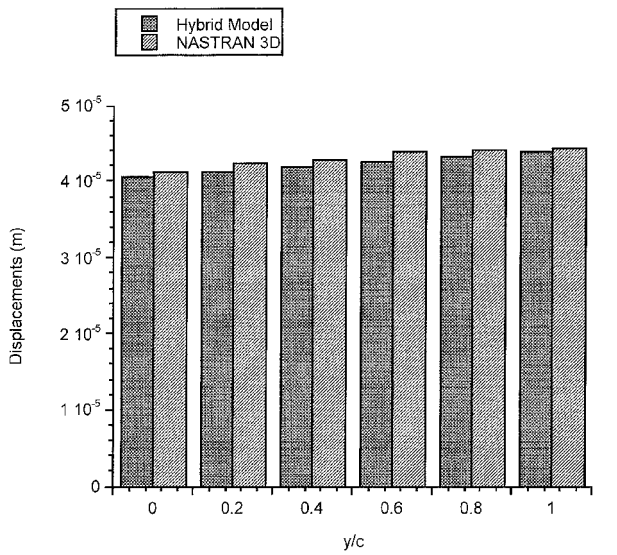

Fig. 8 Tip displacements, case 1.

respectively. The maximum difference in the shear stress values, between the two theories, is on the order of 10%. This is because the present theory is a two-dimensional theory. When the plate thickness is increased ($l/h_c = 20$), as in case 2, the differences in shear stresses calculated by the present method and NASTRAN increase (Fig. 7) as expected. However, the correlations are fairly good considering the present theory is computationally more efficient than three-dimensional analysis. The tip displacements are compared next for the plate. As seen in Fig. 8, the results from the present method correlate extremely well with those obtained using NASTRAN-3D analysis for various locations along plate width (y direction), deviating by a maximum of 1% from the NASTRAN-3D results.

Figure 9 shows the modal comparison for a plate with dimensions $a = 4$ m, $b = 1$ m, $h_c = 0.01$ m, $h_v = 0.00127$ m, and $h_p = 0.00254$ m (case 3). It is seen that the solutions obtained from the present approach are very close to the results predicted using three-dimensional NASTRAN (within 2%). This indicates that the present two-dimensional approach provides accurate prediction

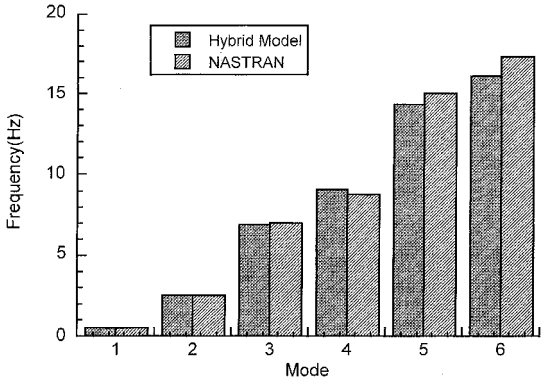

Fig. 9 Natural frequencies; single ACL.

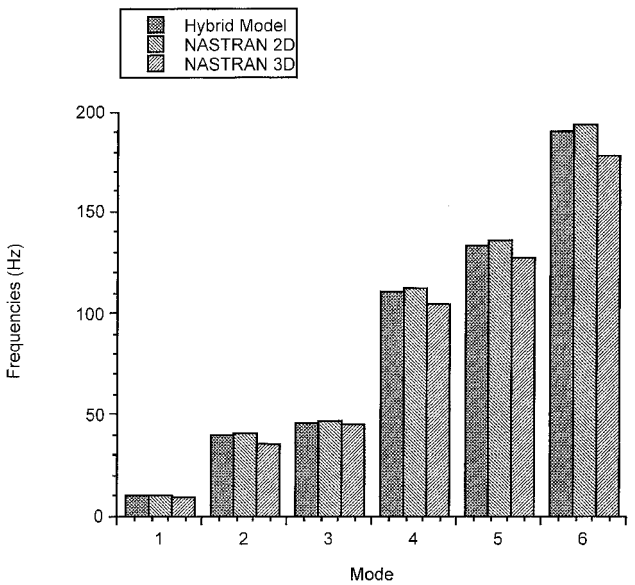

Fig. 10 Natural frequencies; case 2.

in modal analysis comparable to the three-dimensional analysis. Figure 10 shows a comparison of the modal analysis for a thick plate such as the undamped plate specified in case 2 ($l/h_c = 20$). It can be seen that the results from the present approach correlate well with NASTRAN-3D solutions and show an improvement over NASTRAN-2D results (using 100×50 four noded finite element mesh). The results from the present model are within approximately 2% of the results obtained with NASTRAN-3D. Note that NASTRAN is not capable of modeling the constrained layer damping in a structure where active control is applied. It is used here to model the structure without damping effect only for the purpose of correlation. In addition, the use of three-dimensional elements to model composite structures can be very expensive in engineering practice.

Next, dynamic behavior of the cantilevered plate with the same configurations as specified in case 3 is investigated. As mentioned in the preceding section, a pole placement technique is used to design control system for vibration suppression. The target eigenvalues are placed at proper locations by considering the eigenvalues of the passive damper system. Figure 11 shows the eigenvalues of the first six elastic modes of the open-loop system and closed-loop system. The damping ratios of the first four elastic modes of the passive system are 0.1014, 0.0124, 0.0120, and 0.0112. With an active system, the damping ratios are increased to 0.1178, 0.0181, 0.0158, and 0.0121, respectively. It can be seen that damping ratios of all of the lower modes are increased by activating the constrained layer. Time history of tip displacement for the active and passive damper systems are shown in Fig. 12. It is evident that the ACL provides effective attenuation of the vibrations. The corresponding

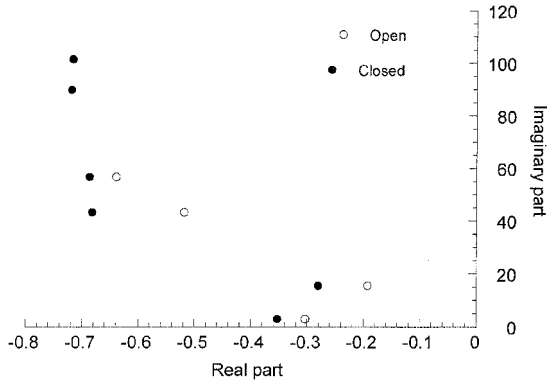

Fig. 11 Comparison of eigenvalues; open and closed loop; single ACL.

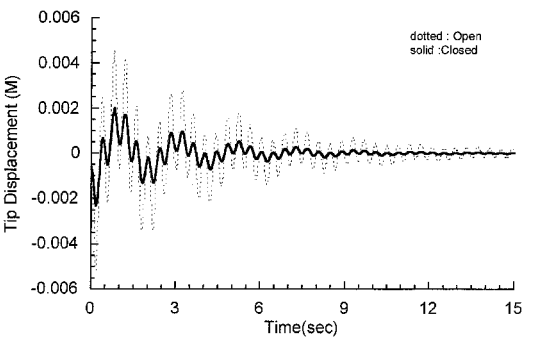

Fig. 12 Time responses of the composite laminate; single ACL.

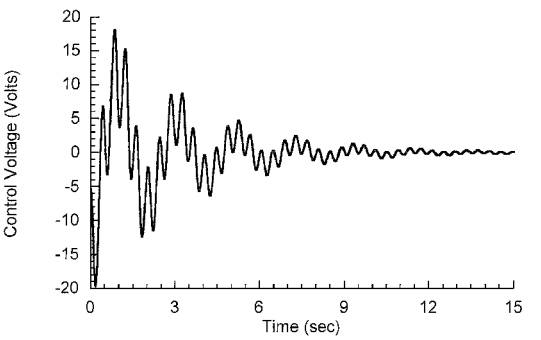

Fig. 13 Control voltage history; single ACL.

control voltage is also plotted in Fig. 13. It can be seen that the damping ratio is increased with the maximum control voltage of only 20 V.

For comparison of the control performance, an example of the cantilevered plate with a pair of ACLs on the top and bottom surfaces is also considered. The plate configuration is as identified in case 3. Figure 14 shows tip displacement of the composite laminate with a pair of ACLs. It can be seen that the active system of plate model with a pair of ACLs shows faster response time and substantial reduction in vibration modes, compared to the case with a single ACL (Fig. 12). Note that the model with a pair of ACLs has higher natural frequencies due to increased structural stiffness. The damping ratios associated with the first four elastic modes of the passive system are 0.0201, 0.00849, 0.0513, and 0.0512. The passive damping ratios of the two lower modes are smaller compared to the plate model with a single ACL. By activating the constrained layers, the damping ratios are increased to 0.0917, 0.0111, 0.0568, and 0.0514. Figure 15 shows the control voltage applied to a pair of ACLs. As shown in Fig. 15, the maximum applied voltage is less than 10 V.

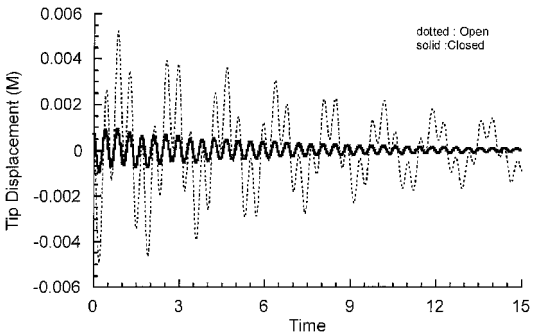

Fig. 14 Time responses of the composite laminate; pair of ACLs.

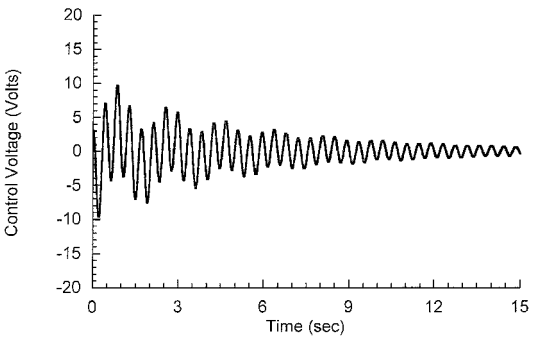

Fig. 15 Control voltage history; pair of ACLs.

Conclusions

A new hybrid displacement field theory is developed to model composite laminates with surface bonded ACL damping. The procedure is implemented using the finite element technique. The higher-order displacement field is used in the composite laminate to capture transverse shear deformations. The first- and the second-order displacement fields are employed in the viscoelastic damping layer and the piezoelectric actuator layer to make the procedure computationally efficient. The developed approach is capable of accurately describing the deformations in the different material regions. It also offers the advantage of having fewer unknown variables in the formulation (only two additional unknown variables compared to the regular refined third-order theory), while satisfying all boundary and continuity conditions. An added benefit is that the boundary conditions for the two additional unknowns, defined in the segmented constraining layer, can also be derived using the present approach. Compared to NASTRAN, the proposed approach is capable of modeling the ACL damping while being efficient and accurate. The anelastic displacement field method is used to implement the viscoelastic material model to enable time-domain finite element analysis. The following specific observations have been made from this study:

1) The developed hybrid displacement field theory is capable of accurately predicting the mechanical behavior of smart composite laminates with varying material layers.

2) The finite element procedure is computationally efficient.

3) The numerical results from the present approach show excellent correlations with NASTRAN-3D finite element solutions, as evidenced by the stress, displacement, and frequency comparisons.

4) Numerical results exhibit significant improvements in active control using the ACL damping treatment.

Acknowledgment

The research was supported by the U.S. Army Research Office, Grant DAAH04-96-1-0163, Technical Monitor, Gary Anderson.

References

[1]Ro, J., and Baz, A., "Optimum Design and Control of Active Constrained Layer Damping," *Journal of Mechanical Design and Journal of Vibration and Acoustics* (special combined ed.), Vol. 117, June 1995, pp. 135–144.

[2]Baz, A., and Ro, J., "Partial Treatment of Flexible Beams with Active Constrained Damping," *Conference of the Society of Engineering Science (ASME-AMD)*, Vol. 167, 1993, pp. 61–68.

[3]Baz, A., and Ro, J., "Finite Element Modeling and Performance of Active Constrained Layer Damping," *Proceeding of 9th VPI&SU Conference on Dynamics and Control of Large Structures*, Virginia Polytechnic Inst. and State Univ., Blacksburg, VA, pp. 345–358.

[4]Van Norstrand, W. C., and Inman, D. J., "Finite Element Model for Active Constrained Layer Damping," *Proceedings of the 31st Society of Engineering Science Meeting: Active Materials and Smart Structures*, Society of Photo-Optical Instrumentation Engineers, Bellingham, WA, Vol. 2427, 1994, pp. 124–139.

[5]Lesieutre, G. A., and Mingori, D. L., "Finite Element Modeling for Frequency-Dependent Materials Using Augmenting Thermodynamic Fields," *Journal of Guidance and Control*, Vol. 13, No. 6, 1990, pp. 1040–1050.

[6]Lam, M. J., Saunders, W. R., and Inman, D. J., "Modeling Active Constrained-Layer Damping Using Finite Element Analysis and GHM Damping Approach," *Proceedings of Conference on Smart Structures and Materials: Passive Damping*, edited by C. D. Johnson and L. C. Rogers, Vol. 2445, Society of Photo-Optical Instrumentation Engineers, Bellingham, WA, 1995, pp. 86–97.

[7]Shen, I. Y., "Bending and Torsional Vibration Control of Composite Beams Through Intelligent Constrained Layer Treatment," *Proceedings of Conference on Smart Structures and Materials: Passive Damping*, edited by C. D. Johnson and L. C. Rogers, Vol. 2445, Society of Photo-Optical Instrumentation Engineers, Bellingham, WA, 1995, pp. 110–122.

[8]Shen, I. Y., "Bending-Vibration Control of Composite and Isotropic Plates Through Intelligent Constrained Layer Treatment," *Journal of Smart Materials and Structures*, Vol. 4, No. 2, 1995, pp. 59–70.

[9]Shen, I. Y., "Hybrid Damping Through Intelligent Constrained Layer Treatment," *Journal of Vibration and Acoustics*, Vol. 116, No. 3, 1994, pp. 341–349.

[10]Shen, I. Y., "Stability and Controllability of Euler–Bernoulli Beams with Intelligent Constrained Layer Treatment," *Journal of Vibration and Acoustics*, Vol. 118, No. 1, 1996, pp. 70–77.

[11]Azvine, B., Tomlinson, G. R., and Wynne, R. J., "Use of Active Constrained-Layer Damping for Controlling Resonant Vibration," *Journal of Smart Materials and Structures*, Vol. 4, No. 1, 1995, pp. 1–6.

[12]Liao, W. H., and Wang, K. W., "On the Active–Passive Hybrid Control Actions of Structures with Active Constrained Layer Treatment," *Proceedings of ASME 15th Biennial Conference on Mechanical Vibration and Noise*, DE Vol. 84-3, American Society of Mechanical Engineers, Fairfield, NJ, 1995, pp. 125–141.

[13]Liao, W. H., and Wang, K. W., "A New Active Constrained Layer Configuration with Enhanced Boundary Actions," *Journal of Smart Materials and Structures*, Vol. 5, No. 5, 1996, pp. 638–648.

[14]Lesieutre, G. A., and Lee, U., "A Finite Element for Beams Having Segmented Active Constrained Layers with Frequency-Dependent Viscoelastics," *Journal of Smart Materials and Structures*, Vol. 5, No. 5, 1996, pp. 615–627.

[15]Cavin, R. K., III, and Bhattacharyya, S. P., "Robust Well-Conditioned Eigenstructure Assignment via Sylvester's Equation," *Journal of Optimal Control Applications and Methods*, Vol. 4, No. 3, 1983, pp. 205–212.

[16]Rew, D. W., Junkins, J. L., and Juang, J. N., "Robust Eigenstructure Assignment by a Projection Method: Application Using Multiple Optimization Criteria," *Journal of Guidance, Control, and Dynamics*, Vol. 12, No. 3, 1989, pp. 396–403.

[17]Junkins, J. L., and Kim, Y., *Introduction to Dynamics and Control of Flexible Structures*, AIAA, Washington, DC, 1993, pp. 235–296.

A. M. Baz
Associate Editor